Nitrogen-Vacancy Centers in Diamond *and* Novel Experiments on Temporally Long Biphotons

PHYS 522/ECE 695 Lecture S1 Notes

Joseph M. Lukens

March 3, 2014

1 Introduction

These notes are designed to complement the seminar led by Dr. Chinmay Belthangady during class time on Monday, February 24. Belthangady is currently a postdoctoral researcher in Ronald Walsworth's group at Harvard University, and his talk was titled "Quantum-assisted magnetometry with NV centers in diamond." My focus in these notes is to introduce the basics of nitrogen-vacancy (NV) centers in diamond, discussing their key properties and capabilities—in particular for high-precision measurements of magnetic fields. Where appropriate I will allude to the specific experiments discussed in Belthangady's seminar, but overall the emphasis will be on building the fundamentals required to understand the literature in this field.

I will then shift gears and discuss Belthangady's previous work on the generation and modulation of entangled photons, experiments he conducted while obtaining his PhD under the direction of Steve Harris at Stanford University. These were mentioned only briefly in the seminar, but since they have proven quite influential in quantum optics, I have decided to include an introduction to them as well.

2 Basics of NV Centers in Diamond

The nitrogen-vacancy (NV) center in diamond is an invaluable system for quantum mechanical experiments, including single-photon generation, quantum computing, and sensitive measurements of the electromagnetic field [1,2]. Such NV centers effectively represent artificial atoms, providing solid-state—and room-temperature—alternatives to trapped ions for investigations of single-atom behavior. A pure diamond lattice consists entirely of carbon atoms joined covalently to their four nearest neighbors; in an NV center, a carbon atom is replaced by nitrogen, with one of the neighboring sites vacant as well. Figure 1 provides a schematic of the lattice structure around an NV. In experiment, the most useful variety is the so-called negative NV center, which consists of six electrons: two are provided by the nitrogen atom (since the other three valence electrons are bonded to carbon atoms); three are unbound electrons from the vacancy site; and one more is obtained from a nitrogen donor, as frequently nitrogen defects form in the lattice without an adjacent vacancy, leaving an extra electron not bound to the adjoining carbons [2]. Although neutral and positive NV centers are also achievable, these do not possess the favorable optical and magnetic properties of negative NV centers. Therefore in the remainder of these notes, negative NV is assumed unless specified otherwise.

The key properties of NV centers which furnish the basis for their extensive use can be gleaned from the simplified energy-level diagram provided in Fig. 2 [2]. The electronic ground state $|g\rangle$ is a spin triplet, with three possible projections of the spin quantum number m_s: $-1, 0, 1$. The surrounding crystal field raises the energy of the $m_s = \pm 1$ states by 2.87 GHz compared to the $m_s = 0$ state, and any additional magnetic field will cause splitting of the $m_s = \pm 1$ sublevel through the Zeeman effect. Since this energy difference is directly proportional to the magnetic field B, this behavior represents the foundation for NV-center-based magnetometers—devices that measure magnetic field strength. Transitions to the excited triplet states $|e, m_s\rangle$ can be achieved through optical absorption of photons around 1.945 eV (638 nm); since this process preserves spin, each of the three ground states can only be excited to states with like values of the spin projection number m_s. But once excited, the most probable mechanism for relaxation varies significantly between the $m_s = 0$ and $m_s = \pm 1$ cases. The $|e, m_s = \pm 1\rangle$ states are strongly—and non-radiatively—coupled to an intermediate singlet state, which itself subsequently decays back to the $m_s = 0$ ground state. In

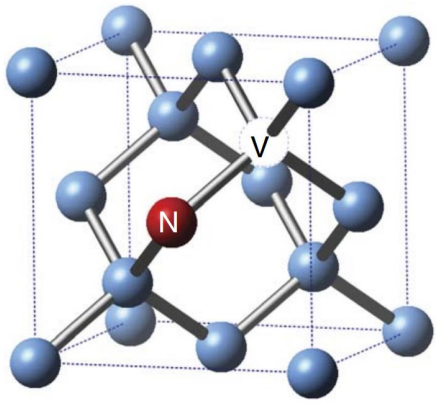

Figure 1: Lattice structure surrounding an NV center. One carbon atom is replaced by a nitrogen atom, and an adjacent site is empty (the vacancy). Image borrowed from Ref. [3].

this way electrons excited to the $|e, m_s = \pm 1\rangle$ levels are significantly likely to relax through a non-radiative process. On the other hand, the $|e, m_s = 0\rangle$ excited state is only weakly coupled to the intermediate singlet; therefore it will most likely decay back to the ground state by emitting a photon.

This divergent behavior offers a means for optical readout of the spin state, a process called optically detected magnetic resonance (ODMR). For if the $|g, m_s = 0\rangle$ ground state is originally occupied, and the NV optically excited by a 1.945-eV laser, the probability of fluorescence is appreciably higher than if one of the $|g, m_s = \pm 1\rangle$ states were initially occupied instead. Specifically, a fluorescence contrast of 30% is obtained [2], allowing the spin state to be read out by simply comparing the rate of detected fluorescence photons. Moreover, driving with the same laser field also permits optical *initialization* of the spin state. Since the $|e, m_s = \pm 1\rangle$ excited states can decay to the $m_s = 0$ ground state, whereas the excitation and relaxation pathways from this ground state do not couple to $m_s = \pm 1$ states, after a sufficiently long laser pulse all electrons will find themselves in $|g, m_s = 0\rangle$, providing a known initial state. Such optical initialization and readout make NV centers particularly amenable to experiment, permitting direct resolution of the relative population levels in the $m_s = 0$ and $m_s = \pm 1$ spin manifolds. Coupled with Zeeman splitting, the stage is set for NV-based magnetometry,

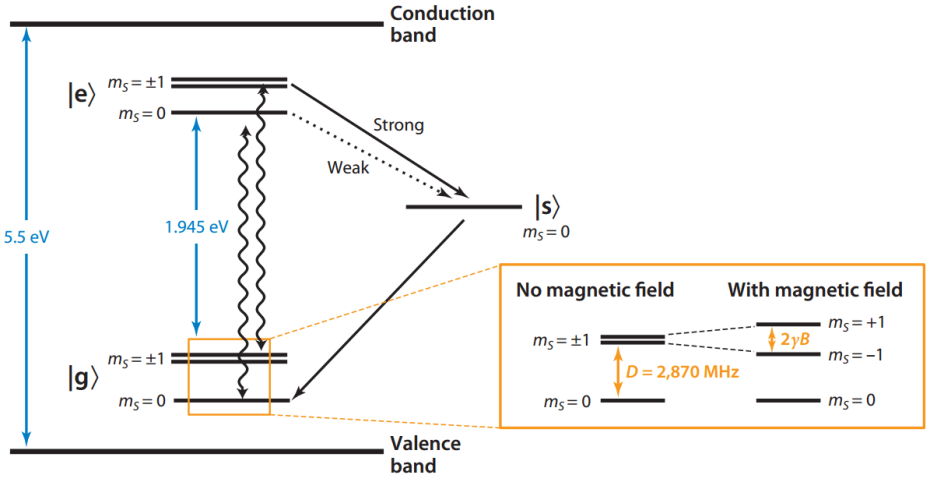

Figure 2: Simplified electronic energy levels for an NV center. Drawing taken from Ref. [2].

the subject of the next section.

3 Magnetometry Based on NV Centers

As emphasized by Belthangady in his talk, magnetometers should ideally possess two key qualities: high sensitivity and high spatial resolution. High sensitivity is necessary to resolve very weak magnetic fields, whereas good spatial resolution is required for measurement of the field distribution on short length scales. Yet most magnetometer designs cannot simultaneously optimize both qualities; for example, while a superconducting quantum interference device (SQUID) can offer femtotesla magnetic field resolution (for 1-s averaging), doing so at the sub-micron level is not possible. NV centers, on the other hand, offer the potential to achieve high sensitivity and resolution *simultaneously*, due to their atomic-scale size [4]. And so in this section, I will discuss the basic techniques for NV-center magnetometry, highlighting some of the key experimental demonstrations as well.

All magnetic measurement techniques make use of the Zeeman splitting of the $|g, m_s = \pm 1\rangle$ sublevel and employ some form of optical readout to measure the relative populations of the spin manifolds. The simplest—

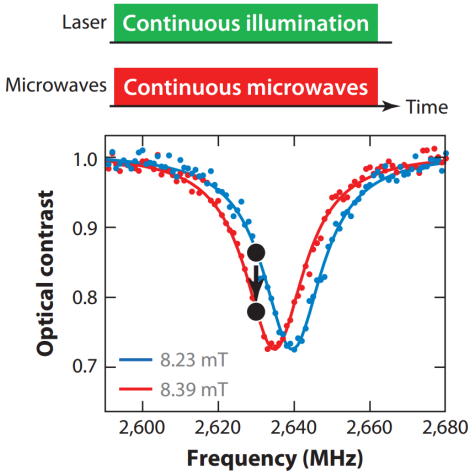

Figure 3: Example of resonance shifting in the presence of an external magnetic field. The microwave frequency at which the fluorescence dips is directly related to the applied magnetic field. Figure borrowed from Ref. [2].

and least sensitive—approach combines continuous-wave optical illumination with a frequency-swept microwave field [2]. When the microwave frequency is far from transition frequencies between spin levels, the electrons promoted by the optical field to the $|e, m_s = 0\rangle$ level fluoresce back to the $m_s = 0$ ground sate; they do not cross over into $m_s = \pm 1$ states. However, when the microwave frequency matches a transition from $|g, m_s = 0\rangle$ to $|g, m_s = -1\rangle$ or $|g, m_s = 1\rangle$, an appreciable fraction of the electrons are excited to the $|g, m_s = \pm 1\rangle$ manifold, after which they can be optically excited to $|e, m_s = \pm 1\rangle$, decaying non-radiatively back to $|g, m_s = 0\rangle$. This increase in non-radiative relaxation processes manifests itself in a reduced fluorescence rate, confirming that the microwave frequency has tuned to a spin transition, from which the magnetic field can be determined. Figure 3 provides an example of this technique, for the $|g, m_s = 0\rangle$ to $|g, m_s = -1\rangle$ transition under two different static magnetic field strengths. By gauging the shift in resonant frequency, the fields in this example are found to differ in strength by 160 μT.

Although this simple methodology highlights the key physics of NV-center magnetometry, more sophisticated techniques based on microwave pulse sequences can offer vastly improved sensitivity. These approaches were taken

in the experiments covered by Belthangady in the seminar. In all of these examples, the optical field is no longer operated continuously; instead, it is used to initialize the NV center to the $m_s = 0$ ground state, turned off for the microwave excitation sequence, and then reapplied to measure the relative population of the spin sublevels. In the work described by Belthangady, the microwave frequency is chosen to couple the $m_s = 0$ ground state with either the $|g, m_s = 1\rangle$ or $|g, m_s = -1\rangle$ levels (the specific choice is not important), creating an effective two-level quantum system. As is well-known in quantum mechanics (e.g., §6.5 of Ref. [5]), a resonantly driven two-level system displays Rabi oscillations, in which the population oscillates sinusoidally between the two levels. Therefore, if a system initially in the ground state is driven on resonance for a duration equal to one-quarter of a Rabi period (a so-called $\pi/2$ pulse), then the state is left in an equal superposition of the two levels. A pair of such $\pi/2$ pulses forms a Ramsey sequence and can be used for measurements of a static magnetic field, as shown schematically in Fig. 4(a). In this process, the first $\pi/2$ pulse creates a superposition of $m_s = 0$ and $m_s = 1$ (or -1) states. The magnetic field then introduces a phase shift in these states proportional to the field strength and interaction time. Finally, a second $\pi/2$ pulse converts this phase shift to a population difference, which can be read out optically.

The sensitivity of the measurement is maximized by increasing the separation time between the two microwave pulses. In practice, however, it is not possible to increase this arbitrarily, for the coherence time of the NV levels is typically limited to a few microseconds due to interactions with surrounding spins [4]. To significantly increase this coherence time, a more sophisticated Hahn-echo sequence can be used instead; Fig. 4(b) provides an example of how this could work. Halfway between the $\pi/2$ pulses, an additional π microwave pulse (which lasts for half the Rabi period) is inserted. This example shows just one π pulse, although a series of pulses can be employed, in which case the sequence is called n-pulse CPMG, after Carr, Purcell, Meiboom, and Gill. Provided that the magnetic field of interest oscillates at a frequency equal to that of the microwave sequence, its impact on the phase adds cumulatively over all pulses. On the other hand, the perturbing environmental fluctuations—which are in general not matched to this frequency—integrate to zero. With the primary decoherence factors thus nullified, the coherence time of the NV center can be increased by orders of magnitude, approaching the even the millisecond regime [2]. An experimental comparison of the Ramsey and Hahn-echo sequences is given

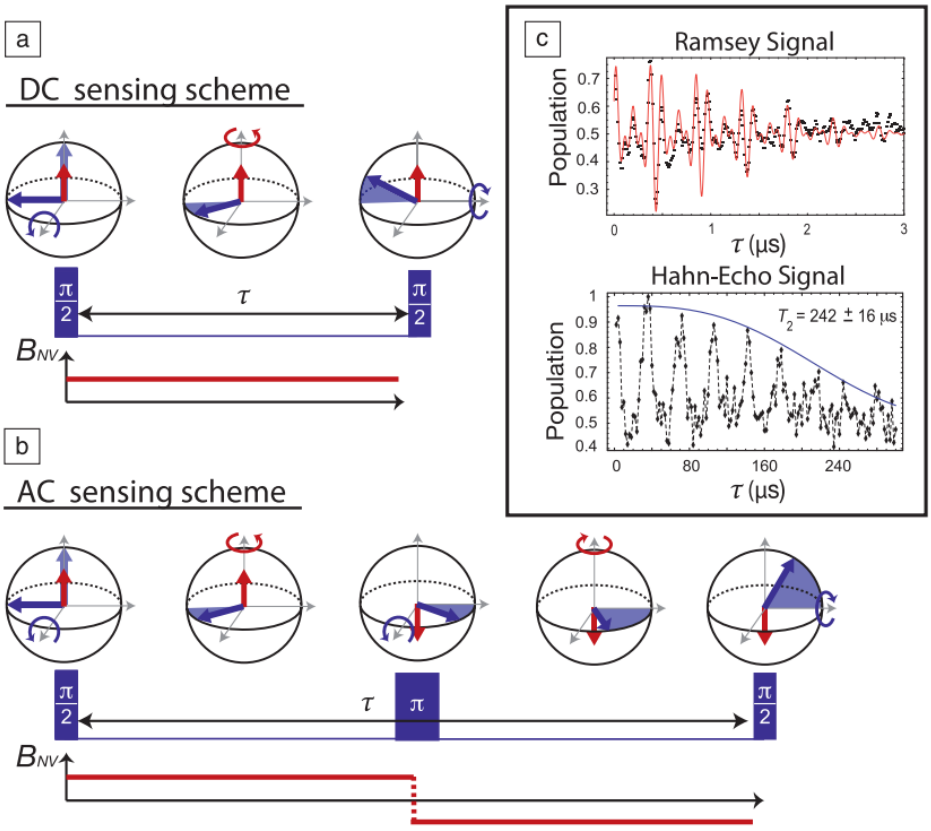

Figure 4: NV-center-based magnetometry with microwave pulse sequences. (a) Schematic of spin precession for a Ramsey sequence. (b) Precession with a Hahn-echo sequence. (c) Experimental comparison of coherence times for both types. The Hahn-echo signal show a coherence time about 100 times longer than the simpler Ramsey sequence. Images from Ref. [4].

Fig. 4(c); the Hahn-echo technique increases the coherence time by two orders of magnitude in this example. Such extended coherence times permit vast improvements in magnetic field sensitivity, yielding values as low as 30 nT $\text{Hz}^{-1/2}$ [6].

To conclude this introduction to NV centers and their application to magnetometry, I will briefly list the journal articles of which Belthangady was a co-author while in Walsworth's group; the reader is directed to them for further information regarding concepts in Belthangady's talk. In Ref. [7], a diamond waveguide was constructed which vastly improves the detection efficiency of fluorescence photons from the NV center. Ref. [3] describes characterization and suppression of the spin-bath environment surrounding NV centers using n-pulse CPMG sequences, also employed in Ref. [8] to achieve extremely long spin coherence times. A technique for synthesizing NV centers with preferential orientations (instead of randomly distributed along all four possible axes) is covered in Ref. [9]. Finally, Ref. [10] demonstrates resonant coupling between NV-center spins and those of substitutional nitrogen defects (i.e., nitrogen atoms without an adjacent vacancy). Since the NV spins can be manipulated optically, whereas the basic nitrogen spins cannot, this method provides a novel means to control these "dark" spins optically. And so it is my hope that this short introduction to NV centers can provide a springboard for the interested reader to examine these papers in greater detail.

4 Generating and Manipulating Temporally Long Biphotons

In this section I cover some of Belthangady's earlier experiments in Steve Harris's group at Stanford, mentioned near the end of the seminar. This work was concerned with the generation and manipulation of entangled photon pairs (or "biphotons") with extremely long correlation times approaching 1 μs. This sits in stark contrast to typical biphoton sources based on spontaneous parametric downconversion in a nonlinear crystal, for unless special design measures are taken, the entangled photons are typically correlated on femtosecond or picosecond time scales. The generation process in Belthangady's experiments to achieve such long correlation times relied on the phenomenon of electromagnetically induced transparency (EIT). As covered in Lecture 6,

sharp changes in the refractive index which occur near resonance are customarily accompanied by strong absorption as well. EIT furnishes a mechanism to render this resonance transparent while still maintaining the large slope of refractive index vs. frequency, through the introduction of a well-chosen pump field. Since the group velocity at frequency ω satisfies

$$v_g = \frac{c}{n} \frac{1}{1 + \frac{\omega}{n} \frac{dn}{d\omega}},$$

where c is the velocity of light in vacuum and n is the refractive index, the large negative slope on resonance can be exploited to produce extremely small group velocities, the basis for so-called "slow light" experiments in which light can be slowed down to near walking speed. For the theory behind EIT and some of the key experiments utilizing it, the reader is directed to §3.8 of Ref. [5] and the references therein.

The energy level diagram for biphoton generation in most of Belthangady's experiments is provided in Fig. 5(a), in which four levels of rubidium are used. The standard EIT experiment would consist of only states $|1\rangle$, $|2\rangle$, and $|3\rangle$, with the pump field at ω_c inducing transparency along the $|1\rangle$-$|3\rangle$ transition (frequency ω_{as}, where as denotes "anti-Stokes"). However, to produce entangled photons, a second, counter-propagating pump at ω_p is introduced as well. Through a spontaneous four-wave mixing process, these two pump fields can mediate the simultaneous production of photons at ω_s (Stokes frequency) and ω_{as}, which propagate in opposite directions to conserve momentum. Because of EIT, the anti-Stokes photon travels extremely slowly through the rubidium cloud, producing biphoton coherence times up to 900 ns, corresponding to a conditional anti-Stokes photon length of 270 m in free space!

These extremely long biphotons can be shaped in interesting ways through electro-optic modulation. An example result is furnished in Fig. 5(b) [11]. In this experiment, detection of the Stokes photon was taken as a trigger for applying a voltage signal to a modulator on the anti-Stokes photon. With no voltage signal, the biphoton correlation function shows a long exponential tail (red curve), but when a pair a square pulses modulates the anti-Stokes field, the correlation function is converted to a set of two peaks (purple curve). These results demonstrate the ability to shape individual photons in the same way as classical pulses. Extending these ideas further, Belthangady and coworkers were able to hide individual photons through modulation techniques borrowed from classical spread-spectrum communications. Figure 6(a)

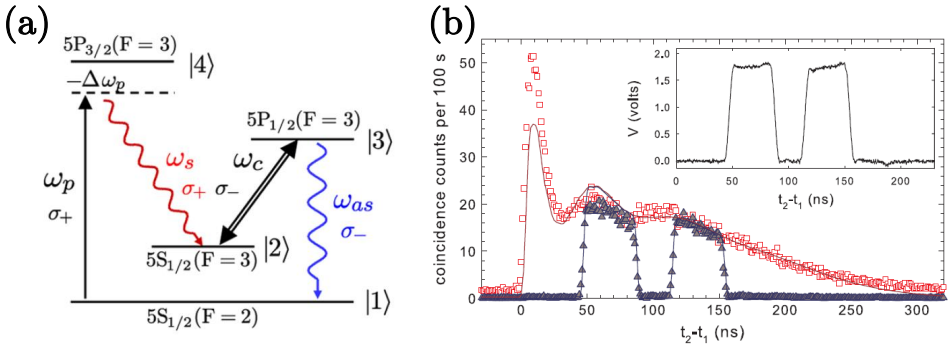

Figure 5: Generation of long biphotons via four-wave mixing in rubidium. (a) Energy level diagram of generation process. (b) Shaping the correlation function with an electro-optic modulator. Taken from Ref. [11].

provides a schematic of this experiment [12]. As before, the Stokes photon is detected as a time reference while the anti-Stokes partner is modulated. Here, though, a pseudorandom binary phase sequence is applied, which has the effect of spreading the biphoton spectrum. Before detection, the anti-Stokes photon is modulated again and passed through a narrowband filter. If the modulation matches the original sequence, the spectrum is despread, and the photon passes through the filter. But if the modulation is not matched, the spectrum remains broad and the photon is most likely blocked by the filter—this idea forms the basis of spread-spectrum communications, which offers resistance to narrowband jamming in classical communication systems.

To show this effect with a single photon, a narrowband laser at the same frequency as the original anti-Stokes photon is injected into the transmission channel; the results are given in Fig. 6(b). With no modulation applied, the characteristic single-photon wavepacket is completely hidden by the more powerful laser field (left panel). Yet turning on both modulators spreads the laser spectrum, blocking it from detection, while ideally having no effect on the doubly modulated anti-Stokes photon; this gives the result in the right panel, revealing the presence of the hidden photon even amid such strong noise in the communications channel. These experiments, along with other work by Belthangady at Stanford (e.g., Refs. [13–16]), highlight some of the fascinating possibilities for this unique biphoton source, in particular in exploring the information potential of single photons.

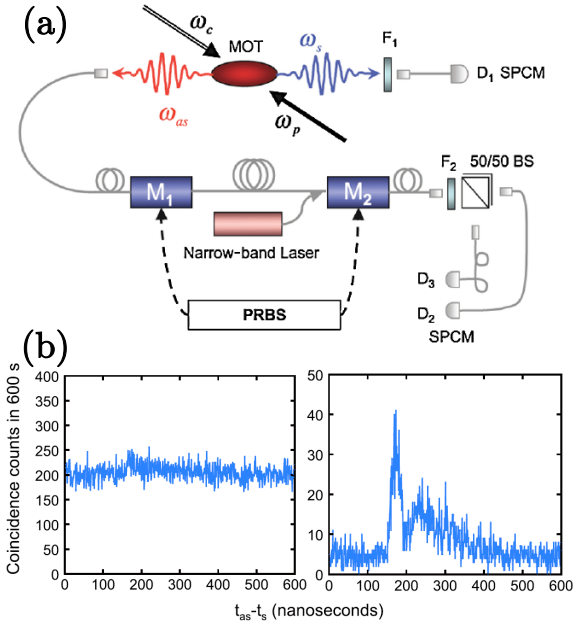

Figure 6: Coding of single photons with electro-optic modulation. (a) Experimental setup. (b) Hiding and recovering single photons. Left: single photon is hidden by the much more powerful laser field. Right: recovering the single-photon wavepacket through matched modulation at the transmitter and receiver. Images borrowed from Ref. [12].

References

[1] V. Acosta and P. Hemmer, MRS Bulletin **38**, 127 (2013).

[2] R. Schirhagl, K. Chang, M. Loretz, and C. L. Degen, Ann. Rev. Phys. Chem. **65**, 83 (2014).

[3] N. Bar-Gill *et al.*, Nature Commun. **3**, 858 (2012).

[4] S. Hong *et al.*, MRS Bulletin **38**, 155 (2013).

[5] R. W. Boyd, *Nonlinear Optics*, 3rd ed. (Academic Press, 2008).

[6] J. P. Maze *et al.*, Nature **455**, 644 (2008).

[7] D. Le Sage *et al.*, Phys. Rev. B **85**, 121202 (2012).

[8] L. M. Pham *et al.*, Phys. Rev. B **86**, 045214 (2012).

[9] L. M. Pham *et al.*, Phys. Rev. B **86**, 121202 (2012).

[10] C. Belthangady *et al.*, Phys. Rev. Lett. **110**, 157601 (2013).

[11] P. Kolchin *et al.*, Phys. Rev. Lett. **101**, 103601 (2008).

[12] P. Kolchin *et al.*, Phys. Rev. Lett. **101**, 103601 (2008).
[13] P. Kolchin *et al.*, Phys. Rev. Lett. **97**, 113602 (2006).
[14] S. Du *et al.*, Phys. Rev. Lett. **100**, 183603 (2008).
[15] S. Du *et al.*, Opt. Lett. **33**, 2149 (2008).
[16] C. Belthangady *et al.*, Phys. Rev. A **80**, 031803 (2009).